

# Cosmological abundances of right-handed neutrinos

KARI ENQVIST<sup>1</sup>, PETTERI KERÄNEN<sup>2</sup>, JUKKA MAALAMPI<sup>3</sup>

and

HANNES UIBO<sup>4</sup>

Department of Physics, P.O. Box 9, FIN-00014 University of Helsinki, Finland

17 August 1996

## Abstract

We study the equilibration of the right-helicity states of light Dirac neutrinos in the early universe by solving the momentum dependent Boltzmann equations numerically. We show that the main effect is due to electroweak gauge boson poles, which enhance thermalization rates by some three orders of magnitude. The right-helicity states of tau neutrinos will be brought in equilibrium independently of their initial distribution at a temperature above the poles if  $m_{\nu_\tau} \gtrsim 10$  keV.

---

<sup>1</sup>enqvist@rock.helsinki.fi;

<sup>2</sup>keranen@phcu.helsinki.fi;

<sup>3</sup>maalampi@phcu.helsinki.fi;

<sup>4</sup>ulbo@phcu.helsinki.fi (on a leave of absence from Institute of Physics, Tartu, Estonia)

# 1 Introduction

Primordial nucleosynthesis is a remarkable probe of neutrino properties [1]. Although recently the increasing accuracy of the cosmological data, such as observations related to the primordial abundances of helium, deuterium and the other light elements, has emphasized systematic errors inherent to primordial nucleosynthesis analysis, there remains a great potential for constraining neutrino physics via cosmological observations. To some extent primordial nucleosynthesis could be sensitive even to the Dirac vs. Majorana nature of neutrinos, because in the Dirac case the small relic abundance of the inert right-handed component of Dirac neutrino would also contribute at nucleosynthesis. Of course, presently one cannot hope to differentiate between the Dirac and Majorana nature of neutrinos on cosmological grounds, but in principle this is an interesting problem. In practise, because of the smallness of the electron neutrino mass, from this point of view only the right-handed components of  $\nu_\mu$  and  $\nu_\tau$  can have interesting relic abundances.

Naively, the cosmological density of light right-handed neutrinos  $\nu_R$  (or rather the right-helicity states of light neutrinos,  $\nu_+$ ) is expected to be very small. If  $\nu_R$ 's ever were in equilibrium, they decoupled very early because of their low capability of interacting. Assuming this took place well above the electroweak phase transition temperature  $T_{EW}$ , at the onset of primordial nucleosynthesis the contribution of the right-handed component of a Dirac neutrino is given by  $\rho_R \simeq [g_*(1 \text{ MeV})/g_*(T_{EW})]^{4/3} \rho_L \simeq 0.044 \rho_L$ , where  $g_*(T)$  is the effective number of degrees of freedom in thermal equilibrium in the temperature  $T$  and  $\rho_L$  is the equilibrium energy density of left-handed neutrino. This assumes that at high temperature we may consider the gas of quarks, leptons, and gauge bosons nearly ideal, which may not be true. A recent lattice simulation [2] of the QCD energy density above the critical temperature has revealed that the actual energy density is some 15% smaller than expected, which might signify the existence of a condensate at high  $T$ . One also assumes that there is no significant entropy production either at the electroweak or QCD phase transitions. Lattice simulations seem to indicate that this is true for QCD, and the latent heat in the electroweak phase transition is also known to be small [3].

The right-helicity states of Dirac neutrinos are not completely inert in the Standard Model [5] but can be produced (and destroyed) in spin-flip transitions induced by the Dirac mass [4, 6] or the neutrino magnetic moment. If the neutrino mass is large enough,  $\nu_+$  would be produced in collisions below the QCD phase transition temperature, resulting effectively in an additional neutrino species at nucleosynthesis. An important source of  $\nu_+$ 's are also the non-equilibrium neutrino scatterings and decays of pions, as was pointed out in [6]. This gives rise to the bound  $m_{\nu_\mu} \lesssim 130 \text{ keV}$  and  $m_{\nu_\tau} \lesssim 150 \text{ keV}$  [8], using  $T_{QCD} = 100 \text{ MeV}$  and assuming that nucleosynthesis

allows less than 0.3 extra neutrino families. This is very restrictive bound for tau neutrinos since, basing on primordial nucleosynthesis arguments, there seems to be no window of opportunity for a sufficiently stable ( $\tau_\nu \gtrsim 10^2$  sec) tau neutrino in the MeV region because of the production of non-equilibrium electron neutrinos in  $\nu_\tau \bar{\nu}_\tau$  annihilations [9].

The actual cosmological density of the right-helicity neutrinos depends not only on the production rate near the QCD phase transition, but also on whether the right-helicity neutrinos had a chance to equilibrate at some point during the course of the evolution of the universe. In this paper we wish to point out that at  $T \lesssim 100$  GeV there is an enhancement of the  $\nu_+$  production rate due to the electroweak gauge boson poles.<sup>1</sup> As a consequence there is a temperature range in which the production rate can exceed the expansion rate of the universe and the right-helicity neutrinos may be brought into thermal equilibrium with other light particles. This will take place if the neutrino mass is sufficiently large. We show that for the tau neutrino the mass limit is about 10 keV, and of the same order of magnitude for the muon neutrino. At the temperature  $T = 1$  MeV the energy density of right-helicity tau neutrinos with a mass of 10 keV is found to be about 6% of the energy density of an ordinary left-helicity neutrinos, i.e. their contribution to the effective number of neutrino species is  $\Delta N_\nu \simeq 0.06$ . The contribution of right-helicity neutrinos with a smaller mass depends, apart from the mass, on their initial energy density above the electroweak scale.

The paper is organized as follows. In Section 2 we will list all tree-level spin-flip reactions where right-helicity neutrinos are produced and discuss their relative importance. We will also demonstrate the  $W$ -pole effect by considering the reactions  $u\bar{d} \rightarrow \nu_+ \tau^+$  and  $\tau^- u \rightarrow \nu_+ d$  as an example for the right-helicity tau neutrino production. In Section 3 we consider the evolution of right-handed neutrino density and describe the numerical method used in solving the Boltzman equation. The results and a discussion is presented in Section 4.

## 2 Right-helicity neutrino production

### 2.1 Processes

We shall consider the production of right-helicity neutrinos in the Standard Model without assuming any new interactions except the Yukawa interactions of the right-handed neutrino with the scalar doublet. The Yukawa coupling is the origin of Dirac neutrino mass and provides a spin-flip operator responsible for the interactions of the right-helicity neutrinos, the probability of the spin flip being proportional to the

---

<sup>1</sup> The question of the cosmic abundance of the right-handed component of Dirac neutrinos was previously studied in [10]. There the pole effect was not considered.

neutrino mass squared. Another source for the spin-flip is neutrino magnetic moment [7], which appears in the Standard Model first at one-loop level and is, therefore, too small to be of any significance for our considerations.

We shall consider light neutrinos with mass less than 0.2 MeV at temperatures between 1 MeV and 100 GeV. Since each right-helicity neutrino introduces in the matrix element a factor  $m_\nu/|\mathbf{p}_\nu|$ , we may safely neglect processes in which more than one right-helicity neutrino is involved. All relevant processes are listed (up to crossing) in Table 1.

There are 68 purely fermionic  $2 \rightarrow 2$  processes in which a right-helicity muon or tau neutrino can be produced. In addition, a right-helicity tau neutrino can also be produced in 11 lepton and quark three-body decays, and the muon neutrino in another set of 11 three-body decays. Since we are especially interested in interactions occurring around the poles of weak gauge bosons, we have to consider also processes involving  $W^\pm$ ,  $Z$  and  $H$ . There are 16 such processes. Finally, there are 3 two-body decays of  $W^\pm$ ,  $Z$  and  $H$  bosons which are capable producing right-helicity muon and tau neutrinos. However, as we will show below, the processes involving gauge or Higgs bosons can be neglected in comparison with the purely fermionic processes.

In what follows, for definiteness, we will consider only processes including right-helicity tau neutrinos. Since we are mainly interested on processes at temperatures above the muon and tau lepton masses, we expect that the results below are roughly valid also for muon neutrinos.

## 2.2 Production rates

Let us consider a  $2 \rightarrow 2$  scattering  $a + b \rightarrow \nu_+ + d$  where one of the final state particles is a right-helicity neutrino. To estimate the relative importance of various processes we approximate the thermally averaged production rate per one  $\nu_+$  by

$$\begin{aligned} \Gamma_+ = & \frac{1}{n_+^{\text{FD}}} \int d\Pi_a d\Pi_b d\Pi_+ d\Pi_d (2\pi)^4 \delta^{(4)}(p_a + p_b - p_+ - p_d) S |\mathcal{M}_{ab \rightarrow +d}|^2 \\ & \times f_a^{\text{FD}} f_b^{\text{FD}} (1 - f_+^{\text{FD}}) (1 - f_d^{\text{FD}}) , \end{aligned} \quad (1)$$

where  $n_+^{\text{FD}}$  is the the equilibrium number density of the right-handed neutrinos,  $d\Pi_i \equiv d^3p_i/((2\pi)^3 2E_i)$ ,  $S$  is the symmetry factor taking into account identical particles in the initial and/or final states, and  $f_i^{\text{FD}}$  are Fermi-Dirac distribution functions.

At high  $T$  the rate Eq. (1) is infrared sensitive to the thermal corrections in the propagators. In general, the structure of the gauge boson propagators at finite  $T$  is complicated because Lorentz symmetry is lost, which results in separate transverse and longitudinal self energies  $\Pi_T(\omega, \mathbf{k})$  and  $\Pi_L(\omega, \mathbf{k})$ . In practise, however, the leading thermal effect arises from small momenta, so that in most cases it is an excellent approximation just to modify the propagators by introducing a Debye mass  $M^2(T) =$

$\Pi_L(\omega, \mathbf{k} = 0)$ , which we approximate by  $M_i^2(T) \simeq M_i^2 + 0.1 T^2$  ( $i = W, Z$ ). (This modification is necessary in t-channel propagators only, since s-channel propagators are not infrared sensitive.) In this approximation external particles or interaction vertices do not receive thermal corrections. Thus the dispersion relations in the thermal distributions in Eq. (1) remain unchanged. Admittedly, this is a simplistic approach, but for our purposes, and for the desired accuracies, this should be sufficient. In fact, in the region of interest the effects due to thermal masses turn out to be very small.

In addition to thermal corrections, we must account for the imaginary parts of the gauge boson propagators, or the widths. This is particularly important for the s-channel. Thermal corrections will generate additional imaginary parts both in the s-channel and t-channel, but at  $T \lesssim 100$  GeV they may safely be neglected.

A technical detail worth pointing out is that for a fixed helicity, the spin-flip matrix elements are not Lorentz-invariant since the direction of the spin picks out a preferred frame of reference, as was emphasized in [6]. Indeed, a Lorentz boost changes the helicity of the particle, so that sometimes a fixed-helicity reaction forbidden in the CM may actually take place in another frame. This means that it is not sufficient to compute matrix elements just in e.g. the CM-frame, but instead one should use a general frame.

The main purpose of this paper is to show that interactions at the weak boson pole may bring the right-helicity neutrinos to thermal equilibrium. To demonstrate this effect, let us consider the t-channel reaction  $\tau^- u \rightarrow \nu_+ d$  and its crossed s-channel reaction  $u \bar{d} \rightarrow \nu_+ \tau^+$ , where  $\nu_+$  is a right helicity tau neutrino. The matrix element for the t-channel process reads

$$\mathcal{M} = \frac{G_F}{\sqrt{2}} V_{ud} R_W(q^2) (-g_{\mu\nu} + \frac{q_\mu q_\nu}{M_W^2}) \bar{u}_\nu \gamma^\mu (1 - \gamma_5) u_\tau \bar{u}_d \gamma^\nu (1 - \gamma_5) u_u, \quad (2)$$

where  $q = p_\tau - p_\nu$ ,  $V_{ud}$  is the appropriate CKM matrix element, and as in s-channel, the propagator gives rise to a term of the form

$$R_W(q^2) = \frac{M_W^2}{q^2 - M_W^2(T) + i\Gamma_W M_W}. \quad (3)$$

As mentioned above, the width  $\Gamma_W$  is important only for the s-channel. Note the  $T$ -dependence in the numerator. The matrix element squared summed over spins of  $\tau^-$  and quarks is then

$$|\mathcal{M}|^2 = G_F^2 |V_{ud}|^2 |R_W(q^2)|^2 (T_{gg} + T_{gq} + T_{qq}), \quad (4)$$

where

$$\begin{aligned} T_{gg} &= 64(p_\tau \cdot p_u)(K_\nu \cdot p_d), \\ T_{gq} &= \frac{32}{M_W^2} \left\{ [m_u^2(p_\nu \cdot p_d) - m_d^2(p_\nu \cdot p_u)] (K_\nu \cdot p_\tau) \right. \end{aligned}$$

$$\begin{aligned}
& - \left[ (p_\tau \cdot p_\nu) - m_\tau^2 \right] \left[ m_u^2 (K_\nu \cdot p_d) - m_d^2 (K_\nu \cdot p_u) \right] \\
& - m_\nu^2 \left[ m_u^2 (p_\tau \cdot p_d) - m_d^2 (p_\tau \cdot p_u) \right] \Big\} , \\
T_{qq} &= \frac{16}{M_W^4} \left\{ (m_\tau^2 - m_\nu^2) (K_\nu \cdot p_\tau) + 2m_\nu^2 \left[ (p_\tau \cdot p_\nu) - m_\tau^2 \right] \right\} \\
& \times \left\{ \left[ m_u^2 + m_d^2 \right] (p_u \cdot p_d) - 2m_u^2 m_d^2 \right\} . \tag{5}
\end{aligned}$$

Here  $K^\lambda \equiv p^\lambda - m s^\lambda$ , with the spin four-vector  $s^\lambda$  for particles with a definite helicity  $h$  given by

$$s^\lambda = h \left( \frac{|\mathbf{p}|}{m}, \frac{E}{m} \frac{\mathbf{p}}{|\mathbf{p}|} \right) . \tag{6}$$

In the ultra-relativistic limit  $K^\lambda$  can be approximated as

$$K^\lambda \simeq 2p^\lambda \text{ for } h = -1 , \tag{7}$$

$$K^\lambda \simeq \frac{m^2}{2|\mathbf{p}|^2} (|\mathbf{p}|, -\mathbf{p}) \text{ for } h = +1 . \tag{8}$$

Accordingly the quantities  $T_{gg}$ ,  $T_{gq}$  and  $T_{qq}$  in Eq. (5) have in the case of  $\nu_+$  production typical sizes given by

$$\begin{aligned}
T_{gg} &\sim m_\nu^2 T^2 , \\
T_{gq} &\sim (m_q/M_W)^2 m_\nu^2 T^2 , \\
T_{qq} &\sim (m_q/M_W)^2 m_\nu^2 T^4 . \tag{9}
\end{aligned}$$

For the production of  $\nu_-$  one has  $T_{gg} \sim T^4$  ,  $T_{gq} \sim (m_q/M_W)^2 T^4$  and  $T_{qq} \sim (m_q m_\tau/M_W^2)^2 T^4$  . For both  $\nu_+$  and  $\nu_-$  at  $T \lesssim M_W$  and in the case of quarks other than the top, the terms  $T_{gq}$  and  $T_{qq}$  can be neglected in comparison with  $T_{gg}$ . The rates for  $\nu_+$  are suppressed by a factor of the order of  $m_\nu^2/T^2$  compared with those for  $\nu_-$ . However, at higher temperatures,  $T \gg M_W$ , the  $T_{qq}$  term starts to dominate the production rate of  $\nu_+$  because of terms not proportional to  $K_\nu$ . Consequently the production rates of  $\nu_+$  are in this case suppressed by a *constant* factor of the order of  $m_q^2 m_\nu^2/M_W^4$ .

The s-channel matrix element can easily be obtained from Eq. (4) by crossing. The thermal rates for both s- and t-channel processes can then be found from Eq. (1). A numerical integration results in the curves displayed in Fig. 1. Here we have for simplicity ignored the small finite temperature effects. It can be seen from the figure that the effect of the pole is spread over a relatively large temperature range. This is a consequence of thermal averaging. Nevertheless, the enhancement in the s-channel is apparent. The results presented in Fig. 1 are for the tau neutrino of mass 20 keV, but they are equally valid for the muon neutrino. In this case the thermally averaged

production rate  $\Gamma_+$  of the s-channel process is seen to exceed in a certain temperature interval the expansion rate of the universe, given by the Hubble parameter

$$H \equiv \frac{\dot{R}}{R} = \left( \frac{8\pi\rho_{\text{tot}}}{3M_{Pl}^2} \right)^{1/2}. \quad (10)$$

Hence, with this reaction alone a 20 keV right-helicity tau (and muon) neutrino would be brought into thermal equilibrium while universe cools through this stage. The complete analysis described in the next section, which is based on solving the Boltzmann equation with all the relevant processes included, confirms this expectation. The pole effects are indeed important for an estimate of the relic density of right-helicity neutrinos.

In addition to fermionic  $2 \rightarrow 2$  scattering processes, at high  $T$  a potential source for  $\nu_+$ 's are  $2 \rightarrow 2$  processes that involve the gauge or the Higgs bosons in the final or initial state (we dub such processes “bosonic”). Let us consider as an example the process  $\tau^-\gamma \rightarrow \nu_+ W^-$ , where the photon couples either to the charged lepton (Compton scattering) or to the W-boson in a three-boson vertex. For comparison, the thermally averaged rate of this process is also displayed in Fig. 1. One can see that it can be neglected even at temperatures around the pole, because there the production rate of the s-channel purely fermionic process is about three orders of magnitude higher.

We have not considered all possible bosonic processes. It is however very plausible that generically among the  $2 \rightarrow 2$  scattering processes only the purely fermionic processes are important, and among these, s-channel dominates over t-channel because of the pole in the s-channel. In what follows, we will always disregard bosonic processes.

The importance of decays is less straightforward to discern. Numerical inspection reveals that the two-body decays listed in the Table 1 can be neglected: their contribution to the total rate is  $\sim \mathcal{O}(10^{-11})$  at  $T \gtrsim 10$  GeV, at lower temperatures their contribution vanishes exponentially. Three-body decays are more important. We find that while the total contribution from three-body decays is negligible at higher momenta,  $|\mathbf{p}_+|/T \gtrsim 3$ , it is as large as few per cents for  $|\mathbf{p}_+|/T \sim 3$  at  $T \lesssim 1$  GeV, increasing up to  $\sim 30\%$  for very small momenta. For such small momenta also  $\nu_+$  production by  $t \rightarrow b\tau^+\nu_+$ , which has its maximal contribution ( $\sim 10\%$ ) around  $T \sim 30$  GeV, is important.

## 3 Evolution of the right-helicity neutrino density

### 3.1 The Boltzmann equation

Our goal is to estimate the relic abundance of the right-helicity neutrinos  $\nu_+$  as a function of time. Of particular interest is the contribution of the right-helicity neutrinos

to the effective number of neutrinos,  $\Delta N_\nu$ , at the onset of primeval nucleosynthesis. To find  $\Delta N_\nu$  one has to determine first the evolution of the phase space distribution of the right-helicity neutrinos  $f_+(|\mathbf{p}_+|, t)$ <sup>2</sup>. Then using a primordial nucleosynthesis code one computes the increase in the primordial  $^4\text{He}$  abundance  $\Delta Y_p$  resulting from the non-zero energy densities of  $\nu_+$  and  $\bar{\nu}_-$  at the nucleosynthesis time. Since  $^4\text{He}$  abundance is a monotonic function of the total energy density of the universe, one can translate  $\Delta Y_p$  back into  $\Delta N_\nu$ , the effective change of the energy density in units of that of massless two-component neutrinos. Without using the NS code one can approximate  $\Delta N_\nu$  as

$$\Delta N_\nu \simeq \rho_{+,n \leftrightarrow p} / \frac{7\pi^2}{240} T_{n \leftrightarrow p} , \quad (11)$$

where the subscript  $n \leftrightarrow p$  refers to the freeze-out of the reactions which transmute protons and neutrons into each other. The justification of this approximation comes from the fact that  $Y_p$  is predominantly determined by the density of neutrons just after the  $n \leftrightarrow p$  freeze-out.

Let us briefly describe the method we have applied for solving the evolution of the right-helicity neutrino density. The evolution of the distribution  $f_+(|\mathbf{p}_+|, t)$  is governed by the Boltzmann equation

$$\left( \frac{\partial}{\partial t} - H|\mathbf{p}_+| \frac{\partial}{\partial |\mathbf{p}_+|} \right) f_+ = \left( \frac{\partial f_+}{\partial t} \right)_{\text{coll}} \quad (12)$$

with the initial condition

$$f_+(|\mathbf{p}_+|, t_0) = f_+^0(|\mathbf{p}_+|) . \quad (13)$$

Instead of time  $t$ , we will consider the cosmic scale factor  $R$  as the independent variable describing the evolution. Eqs. (12, 13) then transform into

$$\left( R \frac{\partial}{\partial R} - |\mathbf{p}_+| \frac{\partial}{\partial |\mathbf{p}_+|} \right) f_+ = \frac{1}{H} \left( \frac{\partial f_+}{\partial R} \right)_{\text{coll}} \quad (14)$$

and

$$f_+(|\mathbf{p}_+|, R(t_0)) = f_+^0(|\mathbf{p}_+|) . \quad (15)$$

Since  $R$  is defined up to a multiplicative constant (only the ratio of  $R$ 's at two different times has physical meaning), one may choose  $R(t_0) = 1$ .

For solving Eqs. (14, 15) it is important that the first-order PDE (14) may be transformed to an ODE by a suitable transformation of the variables  $|\mathbf{p}_+|$  and  $R$ . We use

$$|\mathbf{p}_+| \rightarrow \tilde{p}_+ = |\mathbf{p}_+| \frac{R}{R_0} , \quad (16)$$

---

<sup>2</sup>The arguments of the distribution function  $f_+(|\mathbf{p}_+|, t)$  indicate that we work in the FRW, *i.e.*, spatially isotropic and homogeneous cosmology.



where  $R_0$  is arbitrary but fixed. Then Eq. (14) may be written as

$$R \frac{\partial}{\partial R} \tilde{f}_+(\tilde{p}_+, R) = \frac{1}{H} \left( \frac{\partial \tilde{f}_+}{\partial R} \right)_{\text{coll}}, \quad (17)$$

where, according to (16),  $\tilde{f}_+(\tilde{p}_+, R) := f_+(|\mathbf{p}_+| = \tilde{p}_+ R_0/R, R)$  and a similar relation holds between the collision terms  $(\partial \tilde{f}_+/\partial R)_{\text{coll}}$  and  $(\partial f_+/\partial R)_{\text{coll}}$ . Eq. (17) describes the evolution of  $\tilde{f}_+(\tilde{p}_+, R)$  with an increasing  $R$  for a fixed value of the parameter  $\tilde{p}_+$ . For noninteracting  $\nu_+$ 's, Eq. (17) is solved by  $\tilde{f}_+ = \text{const}$ , which may be translated into the familiar evolution (caused by momentum redshift) of the distribution function of the freely expanding gas of particles,

$$f_+(|\mathbf{p}_+|, R) = \tilde{f}_+^0(\tilde{p}_+ = |\mathbf{p}_+| R/R_0). \quad (18)$$

This equation describes the compression of the distribution function along the momentum axis as  $R$  increases. For ultrarelativistic particles this compression preserves the shape of the distribution function. Interactions will in general introduce distortions in the distribution function because of the momentum-dependent strength of the coupling of particles with the ambient matter.

As has been already mentioned in Sec. 2.1, we are considering ultrarelativistic neutrinos and therefore are justified to neglect all processes involving more than one right-helicity neutrino. Then, as will be shown in the next subsection, neglecting for a moment a slight  $\tilde{f}_+$ -dependence of the Hubble parameter  $H$  and the  $R$ - $T$  relationship, used in calculation of both  $H$  and the collision term, the r.h.s. of the Eq. (17) is linear in the distribution function of right-helicity neutrinos  $\tilde{f}_+$ , and consequently (17) represents a set of uncoupled differential equations for  $\tilde{f}_+(\tilde{p}_+, R)$ , one independent equation for each value of the parameter  $\tilde{p}_+$ .<sup>3</sup> In our computations we followed the evolution of the distribution function at 30 different values ( $\sim$  bins) of  $\tilde{p}_+$  placed at equal distances in the interval  $0 \leq \tilde{p}_+/(100 \text{ GeV}) \leq 10$ . We took into account the weak dependence of  $H$  and  $T(R)$  on  $\tilde{f}_+$  by solving Eq. (17) iteratively, that is, we evaluated these quantities using the value of  $\tilde{f}_+$  obtained in the previous iteration. Because of the smallness of the correction to  $H$  and  $T(R)$  from  $\tilde{f}_+$  the solution converges rapidly and we had to use only 3 iterations.

### 3.2 The collision term

Considering only purely fermionic  $2 \rightarrow 2$  and  $1 \rightarrow 3$  processes, we can write the collision term on the r.h.s. of (17) in the form

$$\left( \frac{\partial f_+}{\partial R} \right)_{\text{coll}} = (C_{2 \rightarrow 2} + C_{1 \rightarrow 3})(1 - f_+) - (C'_{2 \rightarrow 2} + C'_{1 \rightarrow 3})f_+, \quad (19)$$

---

<sup>3</sup> In the general case when one takes into account also processes with more than one right-helicity neutrinos, the r.h.s. is no more linear in  $\tilde{f}_+$  and one arrives at the set of coupled ODEs for  $\tilde{f}_+$ : the evolution of  $\tilde{f}_+(\tilde{p}_+, R)$  and  $\tilde{f}_+(\tilde{p}'_+, R)$ , for  $\tilde{p}_+ \neq \tilde{p}'_+$ , are not independent.

where the coefficients  $C_I$  represent production and  $C'_I$  destruction of  $\nu_+$ , with  $I = 2 \rightarrow 2, 1 \rightarrow 3$ . The explicit expressions for the quantities  $C_{2 \rightarrow 2}$  and  $C_{1 \rightarrow 3}$  are

$$\begin{aligned}
C_{2 \rightarrow 2}(|\mathbf{p}_+|, R) &= \sum_{\text{scatt}} \frac{1}{2E_+} \int d\Pi_a d\Pi_b d\Pi_d (2\pi)^4 \delta^{(4)}(p_a + p_b - p_+ - p_d) \\
&\quad \times S |\mathcal{M}_{ab \leftrightarrow +d}|^2 f_a^{\text{FD}} f_b^{\text{FD}} (1 - f_d^{\text{FD}}) , \\
C_{1 \rightarrow 3}(|\mathbf{p}_+|, R) &= \sum_{\text{dec}} \frac{1}{2E_+} \int d\Pi_f d\Pi_g d\Pi_h (2\pi)^4 \delta^{(4)}(p_f - p_g - p_+ - p_h) \\
&\quad \times S |\mathcal{M}_{f \leftrightarrow g+h}|^2 f_f^{\text{FD}} (1 - f_g^{\text{FD}}) (1 - f_h^{\text{FD}}) , \quad (20)
\end{aligned}$$

where, as before,  $d\Pi_i \equiv d^3p_i / ((2\pi)^3 2E_i)$  and  $S$  is a symmetry factor taking into account identical particles in the initial and/or final states. Note that these expressions do not include the factors  $g_i$  representing the number of spin degrees of freedom. According to our convention these factors are included already into the matrix elements squared since we sum over polarization states of all particles except the right-helicity neutrino under consideration. We have also used the well justified assumption that charged leptons, quarks and left-helicity neutrinos have thermal FD distributions.

The expressions for  $C'_I$  can be obtained from (20) by the replacement

$$f_i^{\text{FD}} \leftrightarrow (1 - f_i^{\text{FD}}) . \quad (21)$$

Using (20) and (21) one easily finds that the primed and unprimed coefficients are related to each other by

$$C'_I = e^{E_+/T} C_I , \quad (22)$$

where we have assumed that all the particles except the right-helicity neutrino are at a common temperature  $T$  and the chemical potentials of all the particles can be neglected. With Eq. (22) we are able to rewrite (19) in the more compact form

$$\left( \frac{\partial f_+}{\partial R} \right)_{\text{coll}} = (C_{2 \rightarrow 2} + C_{1 \rightarrow 3}) \left[ 1 - \frac{f_+}{f_+^{\text{FD}}} \right] , \quad (23)$$

where  $f_+^{\text{FD}} = [\exp(E_+/T) + 1]^{-1}$ .

Let us introduce the total production rates per unit volume:

$$\begin{aligned}
\Gamma_{2 \rightarrow 2}(R) &= \sum_{\text{scatt}} \int d\Pi_a d\Pi_b d\Pi_+ d\Pi_d (2\pi)^4 \delta^{(4)}(p_a + p_b - p_+ - p_d) \\
&\quad \times S |\mathcal{M}_{ab \leftrightarrow +d}|^2 f_a^{\text{FD}} f_b^{\text{FD}} (1 - f_d^{\text{FD}}) , \\
\Gamma_{1 \rightarrow 3}(R) &= \sum_{\text{dec}} \int d\Pi_f d\Pi_g d\Pi_+ d\Pi_h (2\pi)^4 \delta^{(4)}(p_f - p_g - p_+ - p_h) \\
&\quad \times S |\mathcal{M}_{f \leftrightarrow g+h}|^2 f_f^{\text{FD}} (1 - f_g^{\text{FD}}) (1 - f_h^{\text{FD}}) . \quad (24)
\end{aligned}$$

Note that the expressions given above do not include the blocking factors  $(1 - f_+)$ . Also, the dependence of  $\Gamma_I$ 's on  $R$  arise through the distribution functions of ambient

particles. Comparing Eqs. (20) and (24) one easily sees that

$$\Gamma_I(R) = \int \frac{d^3 p_+}{(2\pi)^3} C_I(|\mathbf{p}_+|, R) , \quad (25)$$

or equivalently

$$C_I(|\mathbf{p}_+|, R) = \frac{d}{d(|\mathbf{p}_+|^3/(6\pi^2))} \Gamma_I(R) . \quad (26)$$

From this expression we see that the quantities  $C_I$ , which are of the dimension of mass, are the production rates of  $\nu_+$ 's per unit volume per unit interval of  $|\mathbf{p}_+|^3/(6\pi^2)$  around  $|\mathbf{p}_+|$ .

Eq. (26) suggests also a general method for calculating  $C_I$ 's. One first generates by a Monte Carlo (MC) method a sample of unweighted events, together with their common weight, such that the total integral over the initial and final state phase space yields  $\Gamma_I$ . Having this sample, the evaluation of the derivative in (26) essentially reduces to building the histogram the number of unweighted events vs.  $|\mathbf{p}_+|^3/(6\pi^2)$ . Although this method is very general (applicable both to scatterings and decays) and with a clear physical meaning, it yields a good accuracy only if one generates the initial sample of weighted events such that there are more weighted events in the regions of the phase space where the integrand in  $\Gamma_I$  is larger. This requires some knowledge of the behaviour of the integrand and an ability to build a MC event generator with the required distribution of events in the phase space.

In the case of  $2 \rightarrow 2$  scatterings there exists also another method of calculation of  $C_{2 \rightarrow 2}$ . This method follows directly from (20) and is based on the T-invariance of interactions allowing to rewrite  $C_{2 \rightarrow 2}$  in a form where  $\nu_+$  is an initial state particle. After this transformation the calculation of the corresponding integral proceeds in a usual way. In order to check our results we have determined  $C_{2 \rightarrow 2}$  with both methods.

### 3.3 Results

The total rates  $C(|\mathbf{p}_+|, R) = C_{2 \rightarrow 2}(|\mathbf{p}_+|, R) + C_{1 \rightarrow 3}(|\mathbf{p}_+|, R)$  for the right-helicity tau neutrino production for a number of fixed momenta are shown in Fig. 2. One can clearly see the effect of the s-channel pole, indicating that the rate is dominated by fermionic s-channel processes. Small momentum states pass through the pole at high temperatures, large at low temperatures. Another feature is the increase of the total rate for very small momentum  $\nu_+$ 's at  $0.2 \text{ GeV} \lesssim T \lesssim 2 \text{ GeV}$ . This enhancement is due to both scatterings ( $u\bar{d} \rightarrow \nu_+ \tau^+$ ,  $c\bar{s} \rightarrow \nu_+ \tau^+$ ) and the decays of the tau lepton. Since at these temperatures the thermally averaged center of mass energy of colliding particles is of the same order of magnitude as the mass of the tau lepton, the neutrinos (and  $\tau$ 's) are preferentially produced in the small-momentum states, for which the probability of the creation of a right-helicity neutrino (spin-flip) is larger. For similar reasons the

contribution of  $\tau$ -decays to the total rate can be as large as  $\sim 30\%$ . For right-helicity muon neutrinos one expects the analogous mechanisms to be effective at temperatures below 100 MeV.

Because different momentum states have different interaction rates, this causes a distortion of the momentum distribution of  $\nu_+$ 's relative to the equilibrium distribution. This effect is demonstrated in Fig. 3. Here we have parametrised the distribution function of  $\nu_+$  for fixed  $R$ ,  $f_+(|\mathbf{p}_+|)$ , introducing a momentum-dependent effective temperature  $T_{\text{eff}}(|\mathbf{p}_+|)$  through  $f_+(|\mathbf{p}_+|) = [\exp(E_+/T_{\text{eff}}(|\mathbf{p}_+|)) + 1]^{-1}$ . In Fig. 3 the ratio  $T_{\text{eff}}/T$  for a tau neutrino of mass 10 keV is shown at  $T = 30, 3$  and  $0.3$  GeV for two extreme initial conditions at a high temperature  $T = 100$  GeV: (i)  $f_+ = f_- = f_+^{\text{FD}}$ , *i.e.* complete equilibrium, and (ii)  $f_+ = 0$ . One sees that only the lowest momentum right-helicity tau neutrinos of this mass will come into full equilibrium at the pole:  $T_{\text{eff}}$  depends on the initial condition even at  $T = 0.3$  GeV for  $|\mathbf{p}_+|/T \gtrsim 1$ . The rise of  $T_{\text{eff}}$  at the small-momentum end of the spectrum is because these states, interacting more strongly, are kept in good thermal contact with ambient matter even when higher momentum states are (already) decoupled. This kind of the distortion of the distribution function becomes more prominent as the mass of the neutrino increases. As mentioned before, the regime of free expansion reveals itself in the shape-preserving evolution of the distribution function. Another remarkable feature is the rise of  $T_{\text{eff}}$  at higher momenta clearly seen for the curve corresponding to  $T = 30$  GeV and the zero initial condition  $f_+ = 0$ . This rise is there despite the fact the total production rate  $C(|\mathbf{p}_+|, R)$  is a monotonically (at least for higher momenta) decreasing function of  $|\mathbf{p}_+|$ . The explanation can be found from Eq. (23): if  $f_+/f_+^{\text{FD}}$  is much smaller than unity, the destruction of  $\nu_+$ 's can be neglected. The regime of well-out-of-equilibrium production of  $\nu_+$  is effectively maintained only while both the interaction rate  $C(|\mathbf{p}_+|, R)$  and the ratio  $f_+/f_+^{\text{FD}}$  are sufficiently small. These conditions are more easily fulfilled by the higher momentum neutrinos at the beginning of their evolution from the zero initial condition. This out-of-equilibrium production results in the distribution function decreasing with  $|\mathbf{p}_+|$  more slowly than the equilibrium distribution function, or, equivalently, an  $T_{\text{eff}}$  rising with  $|\mathbf{p}_+|$ . In contrast with the above discussed rise of  $T_{\text{eff}}$  at lower momenta, the later feature becomes more apparent as the mass of the neutrino decreases. We find that spectral distortion changes the energy density of  $\nu_+$ 's (which were in equilibrium at temperatures above the weak interaction pole) at  $\sim 1$  MeV typically by only a few percent. The major difference between the actual energy density and the naive estimate  $\rho_R \simeq 0.044 \rho_L$  is due to the relatively late decoupling caused by the pole.

Once the initial condition is fixed, we may follow the evolution of the energy density of  $\nu_+$ . In Fig. 4 we show the evolution of the right-helicity neutrino energy density for  $m_{\nu_\tau} = 1, 6$  and  $20$  keV for two different initial conditions. If  $m_{\nu_\tau} = 1$  keV, spin-flip

interactions are too weak to affect the evolution, and the resulting relic abundance at nucleosynthesis is, to a high accuracy, what one would naively expect. However, if  $m_{\nu_\tau} = 20$  keV, spin-flip interactions at the pole are strong enough to equilibrate  $\nu_+$  even if initially  $f_+ = 0$ .

The right-helicity neutrino energy density at about nucleosynthesis time in units of left-helicity neutrino energy density is shown in Fig. 5. We see that almost full equilibration of  $\nu_+$  is obtained at some temperature below 100 GeV if  $m_{\nu_\tau} \gtrsim 10$  keV. We have assumed here that there is no entropy production at QCD phase transition so that the only effect is the dilution of the right-helicity neutrino densities by the appropriate ratios of the effective degrees of freedom before and after the phase transition. We have computed  $\Delta N_\nu$  assuming also that below  $T_{\text{QCD}}$  all interactions can be ignored. While this is a very good approximation for smaller masses ( $m_{\nu_\tau} \lesssim 30$  keV), it has been found [6, 8] that for higher masses out-of-equilibrium scatterings and the decay  $\pi^0 \rightarrow \nu_+ \bar{\nu}_+$  (and the decay  $\pi^+ \rightarrow \mu^+ \nu_+$  in the case of muon neutrinos) produce considerable amounts of  $\nu_+$ . Using the results of [8] we estimate that the non-equilibrium reactions occurring below  $T_{\text{QCD}}$  give an additional contribution to  $\Delta N_\nu$ , to be added to our result shown in Fig. 5, which is approximately 0.003 for  $m_{\nu_\tau} = 30$  keV, 0.012 for  $m_{\nu_\tau} = 60$  keV, 0.03 for  $m_{\nu_\tau} = 100$  keV and 0.15 for  $m_{\nu_\tau} = 200$  keV, adopting  $T_{\text{QCD}} = 150$  MeV. Given the inaccuracy of the determination of  $N_\nu$  from the observational data, at present the pole effect cannot be used to derive an upper bound on the masses of Dirac neutrinos.

We have assumed no other interactions than those present in the Standard Model. Any non-standard interaction above the electroweak scale would affect the initial energy density of the right-handed neutrinos. However, according to our results, if the mass of neutrino is more than about 10 keV, nucleosynthesis is not sensitive to such interactions as their effect will be washed out by equilibration at the electroweak pole region. Because this equilibration is inefficient below neutrino masses in the 1 keV range, the cosmological mass limit of stable Dirac neutrinos is not modified. The increase is at most about 4% as expected naively, depending on the unknown initial density at high temperatures.

## Acknowledgements

The work was supported by Academy of Finland. One of us (P.K.) would like to thank the Finnish Cultural Foundation and its Pohjois-Karjala Foundation for financial support, and another (H.U.) the Nordic Council of Ministers and CIMO for grants. We also wish to thank Kimmo Kainulainen for useful discussions.

## References

- [1] For a recent review, see Subir Sarkar, Oxford preprint OUT-95-16P, hep-ph/9602260.
- [2] G. Boyd *et al.* , *Phys. Rev. Lett.* **75** (1995) 4169.
- [3] K. Enqvist, J. Ignatius, K. Kajantie and K. Rummukainen, *Phys. Rev.* **D45** (1992) 3415.
- [4] G.M. Fuller and R.A. Malaney *Phys. Rev.* **D43** (1991) 3136; K. Enqvist and H. Uibo, *Phys. Lett.* **B301** (1993) 376.
- [5] K.J.F. Gaemers, R. Gandhi and J.M. Lattimer, *Phys. Rev.* **D40** (1989) 309.
- [6] A.D. Dolgov, K. Kainulainen and I.Z. Rothstein, *Phys. Rev.* **51** (1995) 4129.
- [7] K. Fujikawa and R. Schrock, *Phys. Rev. Lett.* **45** (1980) 963.
- [8] B.D. Fields, K. Kainulainen and K. A. Olive, CERN-TH/95-335, UMN-TH-1417/95, hep-ph/9512321 (1995).
- [9] A.D. Dolgov, S. Pastor and J.W.F. Valle, preprint FTUV/98-07, IFIC/96-08, hep-ph/9602233 (1996).
- [10] S.L. Shapiro, S.A. Teukolsky and I. Wasserman, *Phys. Rev. Lett.* **45** (1980) 689.
- [11] D. Buskulic *et al.* (ALEPH collaboration), *Phys. Lett.* **B349** (1995) 585; K. Asamagan *et al.* , *Phys. Lett.* **B335** (1994) 231.

Table 1: Processes, up to crossings, which produce a right-helicity tau neutrino  $\nu_+$ .

| fermionic $2 \rightarrow 2$   | bosonic $2 \rightarrow 2$             | 3 – body decays   | 2 – body decays                      |
|---|---------------------------------------|---|--------------------------------------|
| $\nu_\tau \nu_\tau \rightarrow \nu_+ \nu_\tau$  | $\nu_\tau W^- \rightarrow \nu_+ W^-$  | $\tau^- \rightarrow \nu_+ l_j^- \bar{\nu}_j,$<br>$(l_j^- \bar{\nu}_j = e^- \bar{\nu}_e, \mu^- \bar{\nu}_\mu)$ | $W^+ \rightarrow \tau^+ \nu_+$       |
| $\nu_\tau \nu_j \rightarrow \nu_+ \nu_j, (j = e, \mu)$                                | $\nu_\tau Z \rightarrow \nu_+ Z$      | $\tau^- \rightarrow \nu_+ d_n \bar{u}_m,$<br>$(d_n \bar{u}_m = d \bar{u}, s \bar{u}, s \bar{c}, d \bar{c})$   | $Z \rightarrow \nu_+ \bar{\nu}_\tau$ |
| $\nu_\tau \tau^- \rightarrow \nu_+ \tau^-$  | $\nu_\tau H \rightarrow \nu_+ H$      | $t \rightarrow d_n \tau^+ \nu_+,$<br>$(d_n = b, s, d)$  | $H \rightarrow \nu_+ \bar{\nu}_\tau$ |
| $\nu_\tau f_{\text{ch}} \rightarrow \nu_+ f_{\text{ch}}, (f_{\text{ch}} \neq \tau^-)$ | $\tau^- Z \rightarrow \nu_+ W^-$      | $\bar{b} \rightarrow \bar{u}_m \tau^+ \nu_+,$<br>$(\bar{u}_m = \bar{c}, \bar{u})$                             |                                      |
| $\tau^- \nu_j \rightarrow \nu_+ l_j^-, (j = e, \mu)$                                  | $\tau^- H \rightarrow \nu_+ W^-$      |   |                                      |
| $\tau^- u_m \rightarrow \nu_+ d_n$  | $\tau^- \gamma \rightarrow \nu_+ W^-$ |   |                                      |

## Figure captions

**Figure 1.** Thermally averaged production rates per one right-helicity tau neutrino  $\nu_+$  of mass 20 keV for the s-channel process  $u\bar{d} \rightarrow \nu_+\tau^+$ , the t-channel process  $\tau^-u \rightarrow \nu_+d$  and the bosonic process  $\tau^-\gamma \rightarrow \nu_+W^-$ . The Hubble expansion rate is also shown for comparison.

**Figure 2.** The total production rates (dashed curves)  $C(|\mathbf{p}_+|, R)$  of right-helicity tau neutrinos as functions of the temperature  $T$ . From top to bottom, the rates are given for  $\tilde{p}_+/100 \text{ GeV} = 0.33, 1, 2, 4, 6, 8$  and  $10$ . For comparison the evolution of the Hubble parameter  $H$  is also given (solid curve).

**Figure 3.** The ratio of the momentum-dependent effective temperature  $T_{\text{eff}}$  of the right-helicity tau neutrinos of mass 10 keV to the plasma temperature  $T$  at  $T = 30 \text{ GeV}$ ,  $3 \text{ GeV}$  and  $0.3 \text{ GeV}$ . In each case the solid curve corresponds to the equilibrium initial condition  $f_+ = f_+^{\text{FD}}$ , and the dashed curve to the zero initial condition  $f_+ = 0$  at  $T = 100 \text{ GeV}$ .

**Figure 4.** The evolution of  $\rho_+/\rho_+^{\text{FD}}$  of tau neutrinos as a function of the temperature  $T$  for  $m_{\nu_\tau} = 20 \text{ keV}$  (solid curve),  $6 \text{ keV}$  (dot-dashed curve) and  $1 \text{ keV}$  (dashed curve). The evolution is given for two different initial conditions:  $f_+ = f_+^{\text{FD}}$  and  $f_+ = 0$  at  $T = 100 \text{ GeV}$ .

**Figure 5.** The energy density of right-helicity tau neutrinos  $\nu_+$  in units of the effective number of two-component neutrino species,  $\Delta N_\nu$ , as a function of the neutrino mass.  $\Delta N_\nu$  is calculated at  $T = 3 \text{ MeV}$  (solid curves),  $1 \text{ MeV}$  (dashed curves) and  $0.3 \text{ MeV}$  (dot-dashed curves). For  $m_{\nu_\tau} < 20 \text{ keV}$  the two sets of curves differ by initial conditions at  $T = 100 \text{ GeV}$ .



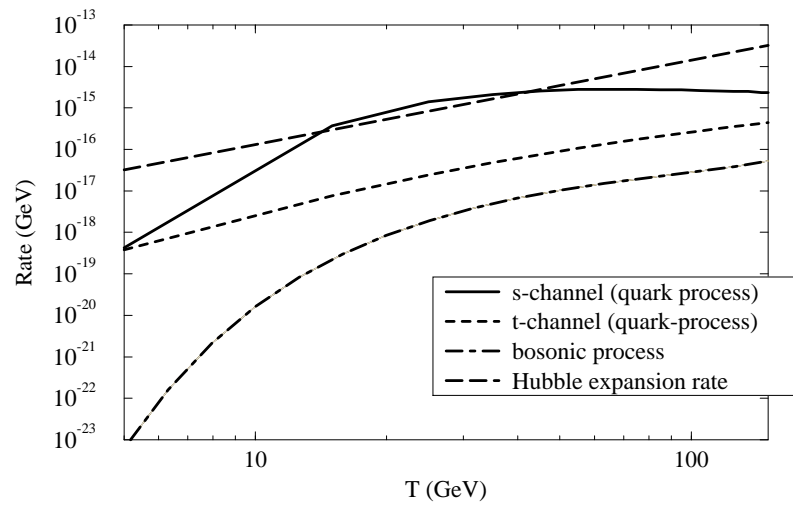


Figure 1

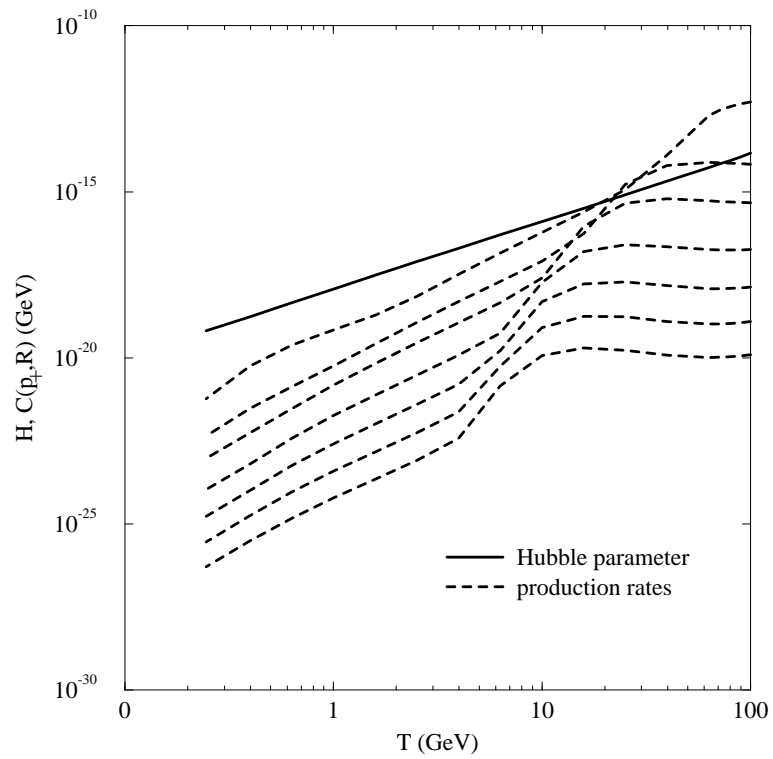


Figure 2

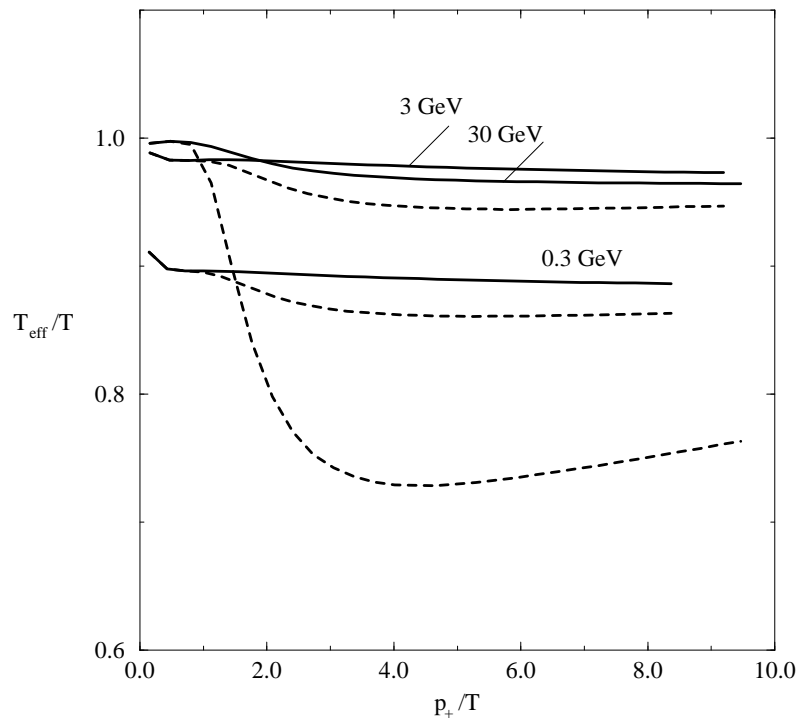


Figure 3

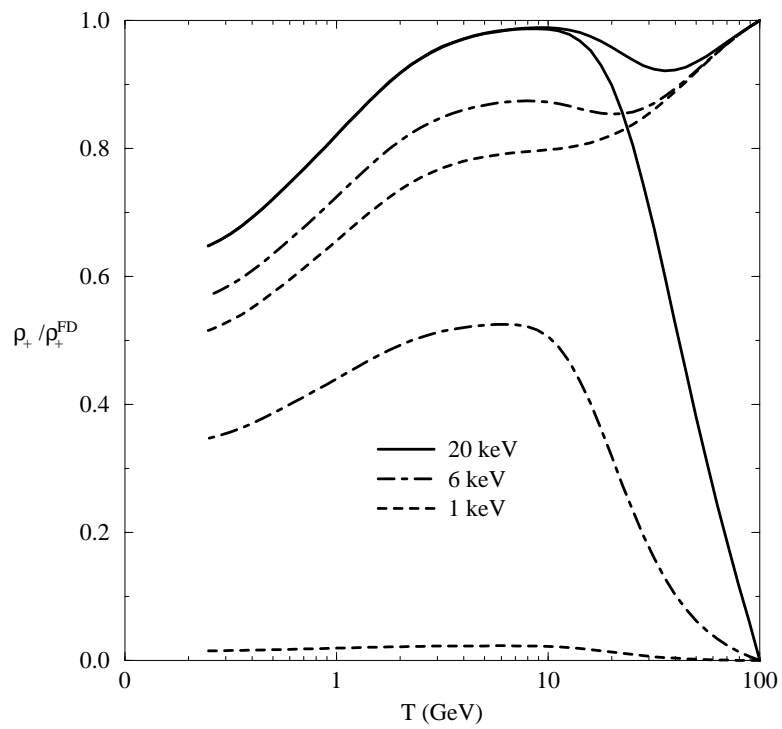


Figure 4

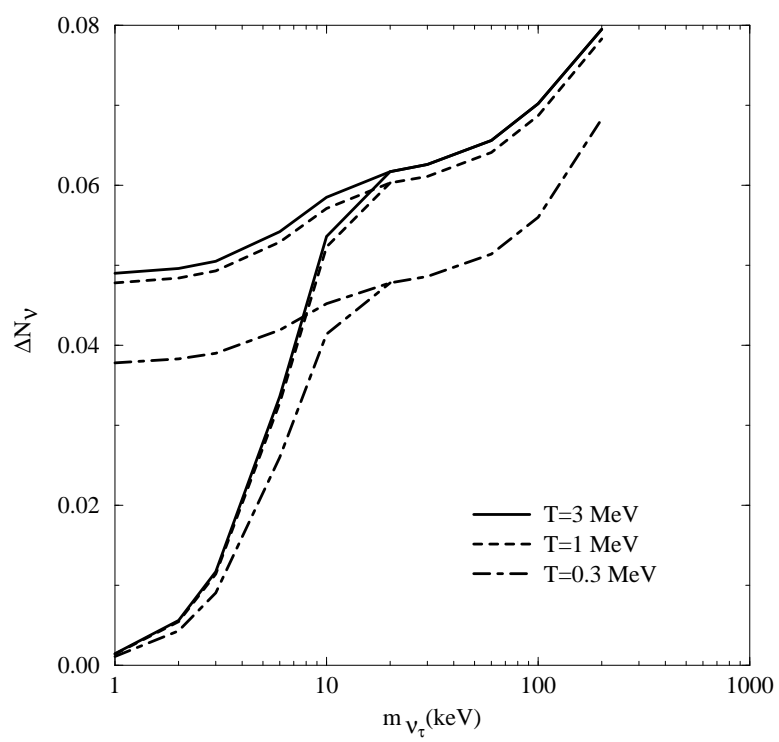


Figure 5